Dynamics of Nonlocal Fisher concentration points: a nonlinear analysis of Turing patterns

Benoît Perthame* Stéphane Génieys †

January 27, 2007

Abstract

The so-called 'nonlocal Fisher' model takes into account an influence neighborhood for inhibition in classical Fisher ecological invasion. In this area, it has been introduced to represent front propagation with redistributed resources. More recently it has also been proposed as the simpler model exhibiting Turing instability and the biological interpretation refers to adaptive evolution. One aspect of the present paper is to propose a nonlinear analysis of these Turing patterns.

More precisely, we introduce a rescaled equation in order to take into account rare mutations (small diffusion). We analyze in which circumstances such a model exhibits stable patterns, among them the Dirac concentrations (that are interpreted as morphs in adaptive dynamics) are remarkable. We use a change of variables, similar to the phase in WKB method, that describes more accurately the phenomenon and leads to a constrained Hamilton-Jacobi equation. It allows us to interpret several features of the patterns, as the weights of the Dirac concentration points, the asymmetry variable regulating their velocities and other relevant quantities.

Key-words Adaptive evolution, Redistributed resources, Turing instability, Nonlocal Fisher equation, Dirac concentrations, Hamilton-Jacobi equation.

1 Model system; the Nonlocal Fisher equation

We consider the periodic solution n_ε to the Nonlocal Fisher equation

$$\begin{cases} \frac{\partial n_\varepsilon}{\partial t}(t) = \varepsilon \Delta n_\varepsilon + \frac{1}{\varepsilon} n_\varepsilon \, (1 - \Phi * n_\varepsilon), \qquad 0 \le x \le 1, \\ \\ n_\varepsilon(t,0) = n_\varepsilon(t,1), \qquad \frac{\partial n_\varepsilon(t,0)}{\partial x} = \frac{\partial n_\varepsilon(t,1)}{\partial x}, \\ \\ n_\varepsilon(t=0,x) = n_\varepsilon^0(x) \ge 0, \end{cases} \tag{1}$$

with an initial data n_ε^0 exhibiting a Dirac mass behavior as we describe it later in more details. The convolution kernel Φ, among other forthcoming properties, has bounded support,

$$\Phi \ge 0, \qquad \int \Phi = 1, \qquad \Phi(x) = 0, \quad \text{for} \quad x \notin [-b, b] \quad (b < \frac{1}{2}). \tag{2}$$

*Département de Mathématiques et Applications, École Normale Supérieure, CNRS UMR8553 , 45 rue d'Ulm, F 75230 Paris cedex 05; Membre de l'Institut Universitaire de France. email: perthame@dma.ens.fr

†Institut Camille Jordan, CNRS UMR 5208, Université Claude Bernard, F69622 Villeurbanne; email: genieys@math.univ-lyon1.fr

This is a rescaled version of the competition model introduced by Génieys, Volpert and Auger [14]. The authors interpret the variable x as a physiological trait, the diffusion term models mutations along with usual genetic population laws (and the scaling means rare mutations with a long range effect). The convolution term mimics competition for resources between individuals whose traits are close enough. But the Nonlocal Fisher equation was also introduced as an ecological model; in the correct range of parameters, it describes an invasion front for a sysytem with redistributed resources, see [16] and the references therein.

The interpretation and the results in [14] make a direct link between evolution theory and Turing's instability. Indeed, this model exhibits both Turing's instability (under specific properties on the kernel Φ that we discuss in Section 5.1) and a phenomenon of evolutionary branching: a monomorphic population (i.e. an initial data with a single Dirac mass) may become dimorphic in order to lower the competition. It is an illustration of Darwin's divergence principle, which is a mechanism of branching due to the competition and can arise even in a constant homogeneous environment [8]. This principle is illustrated numerically by using the cellular automata approach ([1] for instance) or differential systems ([11, 15, 22]). It is mathematically investigated by using a probabilistic approach in [6] and game theory in [17]. Its relevance in physiological contexts is discussed in [18].

The re-scaling we have introduced allows us to identify two length scales: ε for the activation and b for the inhibition, typical of Turing's instability [23, 20]. Even though the model is very simple it allows us to recover a general principle in the topic. For *long rang activation and short range inhibition*, i.e. $b \ll \varepsilon$, we expect front propagation. As $b \to 0$ we recover the classical fisher equation which is well-known to exhibit a traveling wave (see [21, 4] for instance). For b small, traveling waves in a nonlocal Fisher equation is studied in [16].

In the other regime *short range activation and long range inhibition*, we expect pattern formations. This arises from an instability that occurs indeed for certain competition kernels Φ characterized by the fact that their Fourier transform is 'negative enough', as proved in [14] (see also Section 5.1). See also the appendix of the present paper for an estimation of the leading wave length. Even though Turing's instability, and thus pattern formation, are more traditional for systems of parabolic PDEs, notice that convolution models are also commonly used in this area, [19, 9].

Our purpose is to study, in this situation when ε vanishes, wether one can expect the asymptotic expansion

$$n_\varepsilon(t,x) \approx \sum_{i=1}^{I} \rho_i(t)\ \delta(x - x_i(t)). \tag{3}$$

This is indeed the same asymptotic regime than the formalism for adaptive dynamics introduced in [11] and also used in [3, 5] for various models arising in population biology. In this language ([15, 10]), this asymptotic can be interpreted as polymorphism and I denotes the number of different traits that can be represent. The interesting feature here is that this number I is not fixed in advance by opposition to the chemostat problem in [11].

The main questions we wish to answer here are

• Is this expansion (3) always true when Turing's instability occurs?

• Can one predict the densities ρ_i of each morph in terms of the competition kernel Φ?

• Can one predict the 'velocity' of the concentration points $x_i(t)$ in terms of the asymmetry of the competition kernel Φ?

• For steady states situations (with symmetric competition kernel Φ) can one predict the spacing between the concentration points $x_i(t)$, and is it given by the wave length of the linearized equation?

• What is the shape of n_ε in this regime?

This paper uses the Hamilton-Jacobi formalism that was introduced in [11] to predict quantitatively the answers to these questions and explain some apparent paradoxes: one of them is that very 'asymmetric' competition kernels can lead to slower velocities of the points $x_i(t)$ than seemingly 'less asymmetric' kernels. Also, several rules have been derived, still validated on specific examples, for Turing instabilities based on the linearized eigenvalues. Here we recover for instance the rule, already explained, on relative ranges for activators and inhibitors related to waves or patterns. However the linearized eigenvector do not necessarily give a good hint on the wave length of the patterns.

The outline is as follows. We first present the asymptotic theory based on Hamilton-Jacobi formalism. Then we analyze the steady states and answer to most of the questions mentioned above. After that, we give the main parameter that determines the dynamics of the Dirac concentration points. We conclude with several mathematical proofs that we gather in a final section.

2 Asymptotic analysis

In this section, we recall the method introduced in [11] which allows to analyze the limit $\varepsilon \to 0$ and study the concentration effects. It is based on a classical idea which consists in introducing a 'phase' along with the WKB method for oscillations. Here the parabolic aspect leads us to a real phase as in 'front propagation' analysis introduced in [12, 2].

A simple example that motivates the forthcoming analysis is the 'zero temperature maxwellian' $n_\varepsilon = \frac{1}{\sqrt{2\pi\varepsilon}} e^{-|x|^2/(2\varepsilon)}$. It converges to a Dirac mass at $x = 0$, but it is easier to pass to the limit in the quantity

$$\varepsilon \ln(n_\varepsilon) = \frac{-|x|^2}{2} - \frac{\varepsilon}{2}\ln(2\pi\varepsilon) \xrightarrow[\varepsilon\to 0]{} -\frac{|x|^2}{2} \le 0.$$

In the same way, one can handle several Dirac masses. We consider for example

$$n_\varepsilon = \frac{1}{\sqrt{2\pi\varepsilon}} \sum_{i=1}^{I} \frac{\rho_i}{\theta_i} e^{-|x-x_i|^2/(2\varepsilon\theta_i)} \xrightarrow[\varepsilon\to 0]{} \sum_{i=1}^{I} \rho_i(t)\, \delta(x - x_i(t))$$

and

$$\varepsilon \ln(n_\varepsilon) \xrightarrow[\varepsilon\to 0]{} -\min_i \frac{|x-x_i|^2}{2\theta_i} \le 0.$$

With this in mind, we set, following [11, 3, 5],

$$n_\varepsilon(t,x) = e^{\varphi_\varepsilon(t,x)/\varepsilon}, \qquad n^0_\varepsilon(x) = e^{\varphi^0_\varepsilon(x)/\varepsilon}$$

with the property

$$\varphi^0_\varepsilon(x) \xrightarrow[\varepsilon\to 0]{} \varphi^0(x) \le 0, \qquad \max \varphi^0 = 0.$$

Then the points where $\varphi(t)$ vanishes are the Dirac concentrations but their weights are not known by this construction.

Inserting this ansatz in equation (1), we find

$$\begin{cases} \frac{\partial \varphi_\varepsilon}{\partial t}(t) = \varepsilon\Delta\varphi_\varepsilon + |\nabla\varphi_\varepsilon|^2 + \ (1 - \Phi * n_\varepsilon), \\ \\ \varphi_\varepsilon(t=0,x) = \varphi^0_\varepsilon(x), \end{cases} \tag{4}$$

From Theorem 5.3 (see the technical results in the last section), we know that, after extraction of a subsequence if necessary, $\varphi_\varepsilon \to \varphi$ (uniformly, locally in time).

The mass control from below and from above, proved in Theorem 5.1 gives us a first property of the limit φ. Namely

$$\max_x \varphi(t,x) = 0 \qquad \forall t \geq 0. \tag{5}$$

Indeed, would this max be negative, then n_ε would go extinct which is not true; would this max be positive, then by continuity this would be true in an interval and n_ε would blow-up contradicting the finite mass property.

Passing to the limit as ε vanishes in (4), we find the Hamilton-Jacobi equation (H.-J. eq. in short)

$$\begin{cases} \frac{\partial \varphi}{\partial t}(t) = |\nabla \varphi|^2 + r(t,x), \\ \\ \varphi(t=0,x) = \varphi^0(x), \end{cases} \tag{6}$$

and

$$r(t,x) = \lim_{\varepsilon \to 0} \ 1 - \Phi * n_\varepsilon, \tag{7}$$

notice that when $\Phi \in C(\mathbb{R})$ this is a uniform limit and $r(t,\cdot) \in C(0,1)$ (continuous functions) for all times. It is a standard point that the limiting solution φ is not smooth (it is only Lipschitz continuous) and satisfies the H.-J. eq. in the viscosity sense of Crandall-Lions (see [7, 13]). There is a specific difficulty here because the time dependency of r in time is just L^∞ but this is handled also with arguments which are standard by now and we refer the reader to [3, 22] for uniqueness and further mathematical analysis of this problem.

Assuming n_ε converges to the sum of Dirac masses as expressed in (3), we find in (5) and (7):

$$\varphi(t, x_i(t)) = 0, \qquad i = 1, ..., I, \tag{8}$$

$$r(t,x) \equiv 1 - \sum_{i=1}^{I} \rho_i(t)\ \Phi(x - x_i(t)). \tag{9}$$

We recall the interpretation that φ satisfies the *constrained H.-J. eq.* (5), (6). To fulfill the constraint on the *max* imposes to introduce Lagrange multipliers, i.e., free parameters that adapts the right-hand side to these constraints, and these are the weights $\rho_i(t)$. Therefore the system (5), (6), (9) can be seen as a coupled problem. As we know it from [11] there might be several solutions when the max in (5) is attained at multiple points and one expects that an additional information has to be added in this case (and it is an open question to find a convenient criteria). Only in the case where a single maximum point is possible, one can prove uniqueness ([3]).

From the relations (8) and (5), we deduce that $\frac{\partial}{\partial t}\varphi(t, x_i(t)) = \nabla \varphi(t, x_i(t)) = 0$. Therefore we find the fundamental relation

$$r(t, x_i(t)) = 0 \qquad 1 \leq i \leq I. \tag{10}$$

This formula is standard in the theory of adaptive dynamics; r is called the *invasion exponent*. The quantity r_x also appears (see the canonical equation (19) for instance) and is called the *selection gradient* and the points where it vanishes are the so-called *singular points*.

3 Steady state

We begin with the simpler situation when the potential Φ is even. Then, the steady states solutions to (1) are reached as it will be explained in Section 4 (but for 'asymmetric potentials' we cannot hope

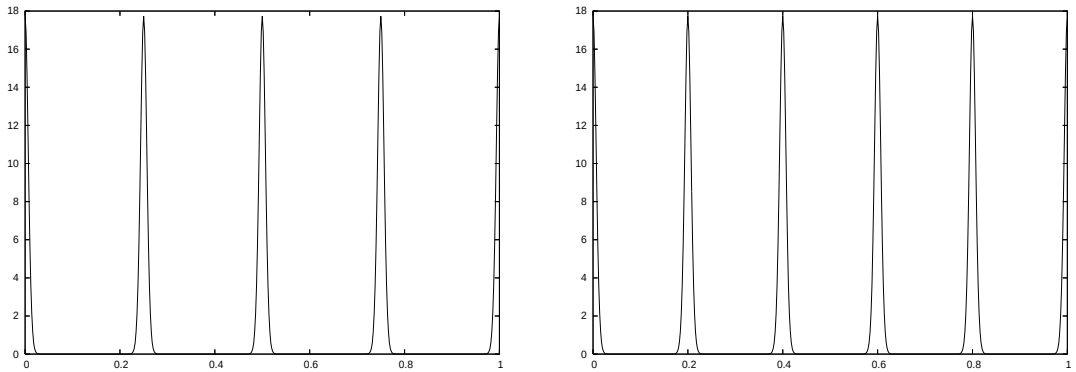

Figure 1: Well-differentiated potential (14) with $a = .015$, $b = .15$, $\varepsilon = 10^{-4}$. Initial conditions are: 4 peaks evenly spaced (left), 5 peaks evenly spaced (right).

for steady states). Then, we have the alternative to study the time asymptotic patterns that satisfy equation

$$\begin{cases} -\varepsilon\Delta n_\varepsilon = \frac{1}{\varepsilon} n_\varepsilon \, (1 - \Phi * n_\varepsilon), \qquad 0 \le x \le 1, \\ \\ n_\varepsilon(0) = n_\varepsilon(1), \qquad \frac{\partial n_\varepsilon(0)}{\partial x} = \frac{\partial n_\varepsilon(1)}{\partial x}. \end{cases} \tag{11}$$

Then, the limiting equation is simpler and reads

$$-|\nabla\varphi|^2 = r(t,x) = 1 - \sum_{j=1}^{I} \rho_j \, \Phi(x - x_j) = \begin{cases} \le 0 \qquad for \quad x \neq x_i, \\ \\ = 0 \qquad for \quad x = x_i. \end{cases} \tag{12}$$

$$\max_x \varphi(x) = 0 = \varphi(x_i), \qquad i = 1, ..., I. \tag{13}$$

We analyze now the numerical results obtained with different *even* competition kernels in view of this asymptotic equation. We have distinguished two cases, both satisfy the Turing instability criteria, but have different behaviors in terms of pattern formation. We refer to them as well- or ill-differentiated.

3.1 Well-differentiated competition

The simplest situation is when we choose a competition kernel exhibiting stronger competition for slightly different traits x (a behavior that is largely accepted and was observed already in [8]). More precisely, we take for real numbers $a > 0$, $b > 0$,

$$\Phi(x) = \Phi(0) \, (1 + a\frac{|x|}{b}) \, \mathbf{1}_{\{|x| \le b\}}, \qquad \int \Phi = 1. \tag{14}$$

On this class of kernels, we have checked numerically that Dirac concentrations are always obtained, and we can discuss the asymptotic prediction made in Section 2.

• (*Location of the concentration points*) Firstly, we observ that the patterns, even though they concentrate as Dirac masses for small ε, depend upon the initial data. Figure 1 exhibits four or five peaks depending on the initial data.

Secondly, we can also check for the example $a = 2$ (but we have tested successfully other values which are not shown here) that the Dirac locations corresponds to the points where $\nabla\varphi$ vanishes; see

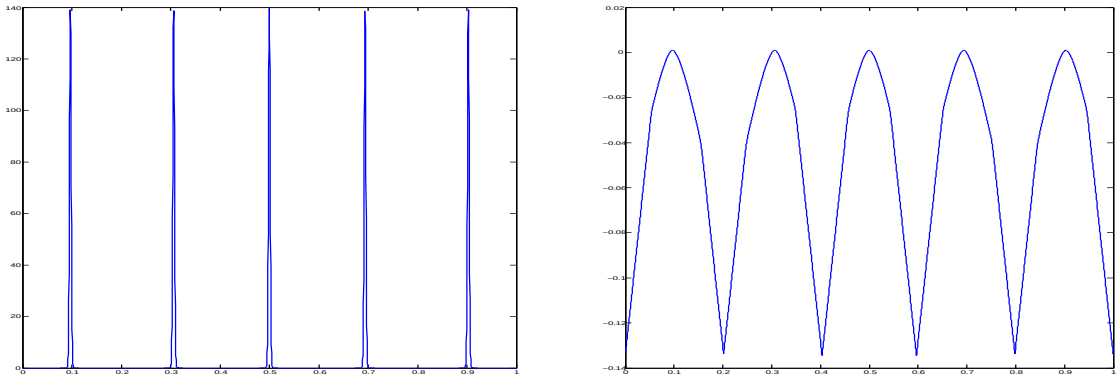

Figure 2: *(Symmetric potential)* Numerical solution of the problem (1) with the well differentiated even potential (14) with $b = .15$, $a = 2$, this corresponds to the third line of Table 1. We represent the density n_ε (left) and the phase φ_ε (right). The numerics is performed with 3000 points, $\varepsilon = 2.10^{-4}$.

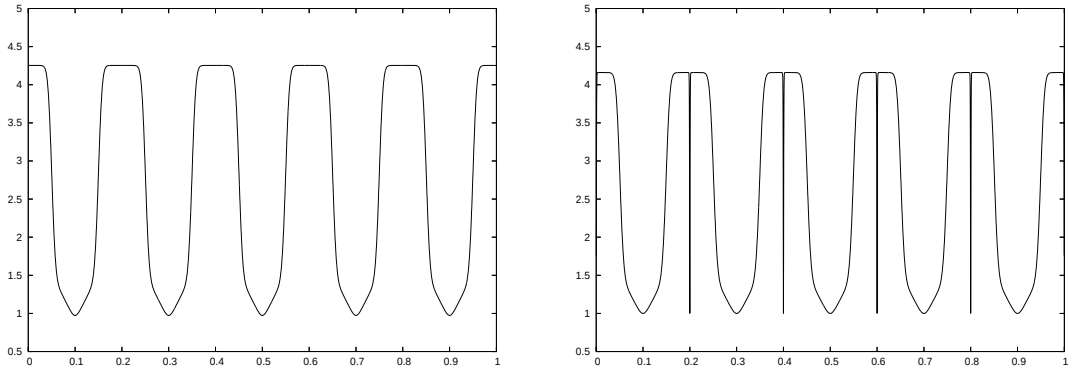

Figure 3: *(Symmetric potential)* Same as Figure 2. We depict the potential $\Phi * n_\varepsilon$ (left) and a centered evaluation of $1 + |\nabla\varphi_\varepsilon|^2$(right).

a	$1/\Phi(0)$	numerical weight
0	.3	.300
1	.45	.442
2	.6	.587
3	.75	.724

a	$1/\Phi(0)$	numerical weight
0	.3	.300
1	.45	.447
2	.6	.594
3	.75	.747

Table 1: *Comparison between the predicted values of the weights of the Dirac mass and the weights obtained by numerical simulations. We have taken the parameter* $b = .15$ *and left:* $\varepsilon = 2\ 10^{-4}$, 3000 *discretization points, right:* $\varepsilon = 5\ 10^{-5}$, 10000 *discretization points,.*

n_ε and φ_ε in Figure 2.

• (*Validity of the H.-J. equation*) Thirdly, we check the validity of the asymptotic limit (5), (6). The Figure 3 depicts the potential $\Phi * n_\varepsilon$ compared to the computed value of $1 + |\nabla\varphi_\varepsilon|^2$. The undershoots are just computational effects when computing the numerical derivative of the solution φ_ε.

• (*Weights of the Dirac masses*) Observe that, in the limiting expression $\Phi * n_\varepsilon = \sum_{j=1}^{I} \rho_j(t)\ \Phi(x - x_j(t))$dis, some overlapping is necessary for $b = .15$ because the values $\Phi * n_\varepsilon(x) = 0$ are unstable. But it occurs on a sufficiently small set in such a way that at the points x_i there is no overlaping. But also, from (12) at the points x_i, we have $\nabla\varphi(x_i) = 0$ (maximum point of φ). Therefore, we predict that the weights ρ_i should satisfy $\rho_i\ \Phi(0) = 1$. The Table 1 shows the computed values ρ_i and compare them to $1/\Phi(0)$. A very good agreement is achieved (to the expense of a very fine grid).

3.2 Ill-differentiated competition

A very interesting case is that initially proposed in [14] where the competition kernel is given by

$$\Phi(x) = \Phi(0)\ \ \mathbf{1}_{\{|x|\le b\}}, \qquad \int \Phi = 1. \tag{15}$$

It is proved in [14] that it exhibits Turing's instability (see also Section 5.1 for an explicit computation in our framework).

It appears, from numerical simulations, that several stable steady states can be produced depending upon the initial data and not all of them converge to Dirac masses as $\varepsilon \to 0$. Here, we only focus on patterns that remain smooth as ε vanishes. Figure 4 shows results indicating that, in place of (3), one should rather expect

$$n_\varepsilon(t,x) \approx \sum_{i=1}^{I} u(x - x_i),$$

where the profile u is a continuous even function with bounded support such that $\int u = 1$. Denoting by c the length of this support, numerical simulations suggest that

$$c + b = \frac{1}{I}. \tag{16}$$

This means that the number of patterns is maximizing space occupation with the property that the potential terms $\Phi * u(x - x_i)$ do not overlap on the support of n_ε, i.e. there is a single i such that

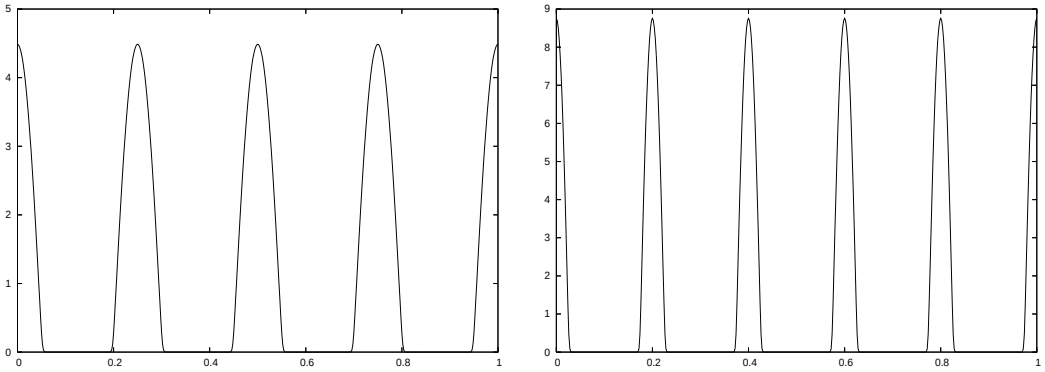

Figure 4: Ill-differentiated potential (15) with $b = .15$, $\varepsilon = 10^{-4}$. Initial conditions are: 4 peaks evenly spaced (left), 5 peaks evenly spaced (right).

$\Phi * u(x - x_i) \neq 0$. In the case of Dirac concentrations, as mentioned earlier some overlapping, away from the x_i's, is also necessary to avoid the state $\Phi * u(x) = 0$ but there is no free parameter c that allows for such an equality since $c = 0$.

Our claim here is that such a steady state is possible only if $c < b$. Indeed similar to the case of Dirac masses, for $x \in [x_i - c/2, x_i + c/2]$, $|\nabla\varphi|^2 = r(t,x) = 1 - \sum_{j=1}^{I} \Phi * u(x - x_j) = 0$ because n_ε remains positive and thus φ vanishes. Since the terms $\Phi * u(x - x_j)$ are non-overlapping on $[x_i - c/2, x_i + c/2]$, this means that

$$\Phi * u(x) \equiv 1, \qquad \text{for } \; x \in [-c/2, c/2]. \tag{17}$$

But for $x \in [-c/2, c/2]$, we can compute $\Phi * u(x) = \displaystyle\int_{\max(x-b,-c/2)}^{\min(x+b,c/2)} u(y)dy$.

If one had $c > b$, for x large enough (say $x \in [b - c/2, c/2]$), we would also have $\Phi * u(x) = \displaystyle\int_{x-b}^{c/2} u(y)dy$ which depends on x and contradicts equation (17). Similarly, for x small enough ($x \in [-c/2, -b + c/2]$), $\Phi * u(x) = \displaystyle\int_{-c/2}^{x+b} u(y)dy$ which contradicts equation (17). On the other hand if $c < b$, $\Phi * u(x) = \displaystyle\int_{-c/2}^{c/2} u(y)dy$ does not depend on x, which is compatible with equation (17).

Hence we have obtained $0 < c < b$ which combined with (16) yields

$$\frac{1}{2b} < I < \frac{1}{b}. \tag{18}$$

Since $I \in \mathbb{N}$, only a finite number of solutions are possible. In the situation of figure 4, we still take $b = .15$ and the numerics is in accordance with the conclusion that steady-states solutions may exist with $I = 4$, 5 or 6. These three possibilities occur, still depending upon the initial data (as in Figure 1).

Notice that for the well-differentiated potentials already presented in Subsection (3.1) we have seen that stable steady states are Dirac masses. Hence the free parameter c is not available to justify

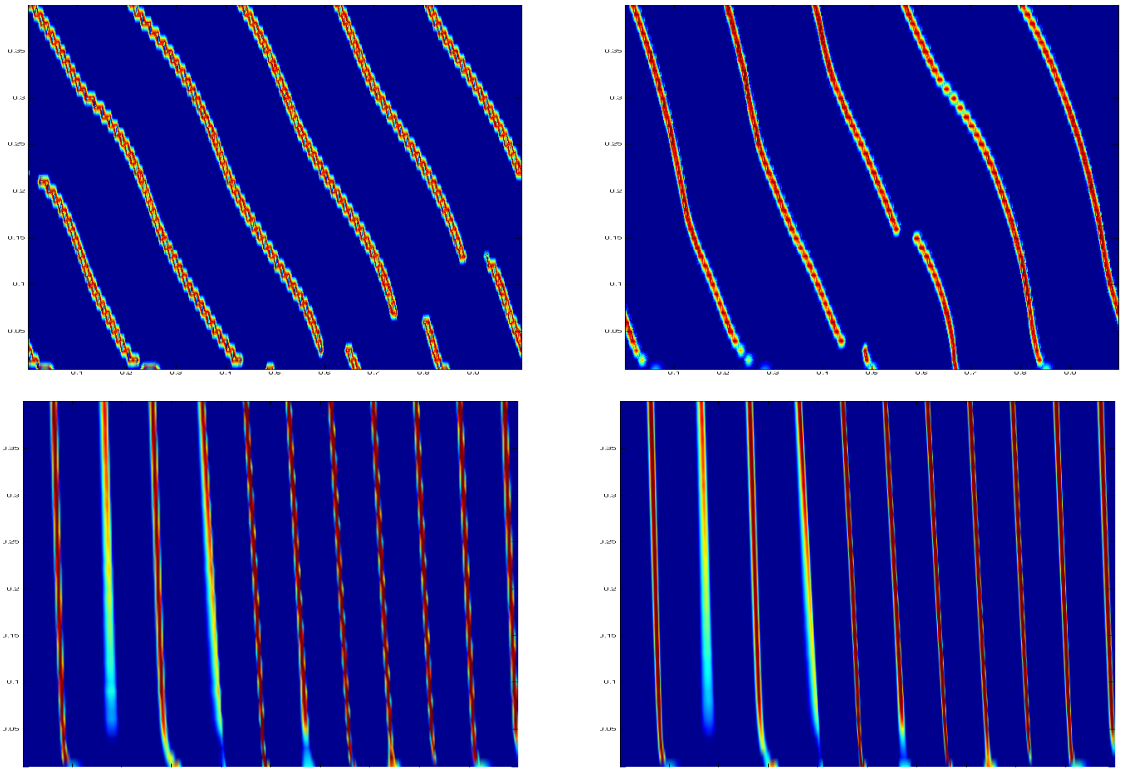

Figure 5: *(Asymmetric potential)* Dynamic of the concentration points with various asymmetric potentials. In the upper left the value $\Phi'(0)$ is larger than in the upper right (a_1 and a_2 respectively). The lower pictures are obtained with an asymmetric potential satisfying $\Phi'(0) = 0$ (potential Φ_3) with 3000 points on the left and 6000 points on the right. The abscissae are x and the ordinates are time.

equation (16). However the numerical simulations of Figure 1 suggest that the possible numbers of peaks are still determined by equation (18).

4 Asymmetry and dynamic of concentration points

We now study the more general case of 'asymmetric' potentials that allow for motion of the concentration points. The question here is to determine which 'asymmetry' criteria controls this motion. A simple and somewhat natural direction would be to measure it by the 'oddness' of the kernel Φ using the quantity $A[\Phi] = \int x\Phi(x)dx$. Our purpose here is to show that the asymptotic theory of Section 2 gives the answer, and it turns out that this 'oddness' quantity $A[\Phi]$ is not the correct one.

Following [11, 22], the H.-J. eq. (6)–(7) contains information on the dynamic of the concentration points $x_i(t)$ defined in the asymptotic formula (3) because they satisfy

$$\phi(t, x_i(t)) = 0.$$

Namely, we recover the velocities with the formula

$$\dot{x_i}(t) = \big(- D^2\varphi(t, x_i(t))\big)^{-1} \frac{\partial r}{\partial x}(t, x_i(t)). \tag{19}$$

and we know from the definition (7), that

$$\frac{\partial r}{\partial x}(t,x) = -\sum_{j=1}^{I} \rho_j(t)\ \Phi'(x - x_j(t)). \tag{20}$$

As a consequence, the correct measure of asymmetry for the speed of the concentration points $x_i(t)$ is given by the quantity $\Phi'(0)$. These points move only when $\Phi'(0) \neq 0$ (and thus Φ is not even).

We check numerically that $x_i(t)$ moves according to the value of $\Phi'(0)$. We have used the three following potentials

$$\Phi_1(x) = a_1(x + .5b)_+ \ \ \mathbf{1}_{\{|x|\leq b\}}, \qquad \int \Phi = 1,$$

$$\Phi_2(x) = a_2(x + b)_+ \ \ \mathbf{1}_{\{|x|\leq b\}}, \qquad \int \Phi = 1,$$

$$\Phi_3(x) = \ \mathbf{1}_{\{-.5b\leq x\leq b\}}, \qquad \int \Phi = 1.$$

We have

$$\Phi_1'(0) > \Phi_2'(0) > \Phi_3'(0) = 0,$$

and thus we can expect that the concentration points move faster for Φ_1 than for Φ_2 and that they do not move with Φ_3. This behavior is indeed obtained as depicted in Figure 5.

5 Mathematical proofs and numerical algorithms

In this section we gather several mathematical results that have been used throughout the paper. They mostly concern a priori estimates. We also describe, for the sake of completeness, the numerical algorithms that we have used.

5.1 Turing's instability and estimation of the typical wave length

For the sake of completeness we reproduce here the computation for deriving the Turing instability condition in model (1), following [14].

Linearizing the equation (1) around the steady state $n = 1$, we obtain

$$\begin{cases} \frac{\partial r}{\partial t}(t) - \varepsilon\Delta r = -\frac{1}{\varepsilon}\Phi * r, \qquad 0 \leq x \leq 1, \\ \\ r(t,\cdot) \ \text{ 1-periodic.} \end{cases}$$

As usual one tries to find solutions with exponential growth, which means eigenvectors

$$\begin{cases} \lambda r(x) - \varepsilon\Delta r = -\frac{1}{\varepsilon}\Phi * r, \qquad 0 \leq x \leq 1, \\ \\ r(\cdot) \ \text{ 1-periodic,} \qquad \lambda > 0. \end{cases} \tag{21}$$

It is natural to decompose a possible solution r in Fourier series

$$r(x) = \sum_{n\in\mathbb{Z}} \widehat{r}(n) e^{2i\pi nx}, \qquad \widehat{r}(n) = \int_0^1 r(x) e^{-2i\pi nx} dx.$$

Then, equation (21) becomes

$$\widehat{r}(n)\big[\lambda + \varepsilon(2\pi n)^2 + \frac{1}{\varepsilon}\widehat{\Phi}(n)\big] = 0.$$

Consequently, the eigenvalues are given by

$$\lambda = -\varepsilon(2\pi n)^2 - \frac{1}{\varepsilon}\widehat{\Phi}(n). \tag{22}$$

Turing instability occurs when some Fourier coefficient of Φ is negative and the leading positive eigenvalue is given for ε small, by

$$\lambda_\varepsilon \approx -\frac{1}{\varepsilon}\min_n \widehat{\Phi}(n) = -\frac{1}{\varepsilon}\widehat{\Phi}(n_0).$$

The corresponding eigenvector is $e^{2i\pi n_0 x}$, which exhibits a wave length $L_0 = \frac{1}{|n_0|}$.

We can specify the example $\Phi = \frac{1}{2b}\ \mathbf{1}_{\{|x|\le b\}}$, with $b < \frac{1}{2}$ and we find that

$$\widehat{\Phi}(n) = \int_{-b}^{b} e^{-2i\pi n x} dx = \frac{1}{2\pi n b}\sin(2\pi n b).$$

The smallest frequency such that instability occurs, $\widehat{\Phi}(n_0) = 0$, is given here by $n_0 = E(\frac{1}{2b}) + 1$ and thus $L_0 = 1/[E(\frac{1}{2b}) + 1]$ (which is close to $2b$ when b is small). This is also the largest possible length of patterns as expressed in (18) but in practice a different wave length is obtained (see Section 3).

5.2 Mass control for the Nonlocal Fisher Eq.

Theorem 5.1 *Assume (2). Then the solution to the Nonlocal Fisher equation (1) has saturated growth and non-extinction. More precisely the total mass $M_\varepsilon(t) = \int n_\varepsilon(t,x)dx$ satisfies*

$$\min\big(M_\varepsilon(0), \frac{1}{\|\Phi\|_\infty}\big) \le M_\varepsilon(t) \le \max\big(M_\varepsilon(0), \frac{1}{\Phi_m c^2}\big),$$

where c and Φ_m are any numbers such that $\Phi \ge \Phi_m$ on $(-2c, 2c)$. Moreover, as $t \to \infty$

$$\liminf M_\varepsilon(t) \ge \frac{1}{\|\Phi\|_\infty}, \qquad \limsup M_\varepsilon(t) \le \frac{1}{\Phi_m c^2}.$$

Remark 5.2 *In view of the numerical experiments, one expects that L^p norms are unbounded for $p > 1$ and ε small in the case of a well-differentiated kernel Φ.*

Proof. (i) Non-extinction. Integrating in x the equation (1), we obtain the relation

$$\frac{d}{dt}M_\varepsilon(t) = \frac{1}{\varepsilon^2}\left(M_\varepsilon(t) - \int n_\varepsilon\ \Phi * n_\varepsilon\right), \tag{23}$$

and we have

$$\Phi * n_\varepsilon \le \|\Phi\|_\infty\ M_\varepsilon(t).$$

Therefore, since $n_\varepsilon \geq 0$, we arrive to the differential inequality

$$\frac{d}{dt}M_\varepsilon(t) \geq \frac{M_\varepsilon(t)}{\varepsilon^2}\left(1 - M_\varepsilon(t)\|\Phi\|_\infty\right),$$

which proves the lower bound.

(ii) Limited growth. Consider a value $c > 0$ as in the statement of Theorem 5.1, and an interval I of length c where

$$\int_I n_\varepsilon dx \geq c\, M_\varepsilon(t).$$

Then, still with the notations in the statement of Theorem 5.1, we have the lower bounds

$$\begin{aligned}\int n_\varepsilon\ \Phi * n_\varepsilon &\geq \Phi_m \textstyle\int_{|x-y|\leq 2c} n_\varepsilon(t,x)\ n_\varepsilon(t,y)\ dxdy \\ &\geq \Phi_m \textstyle\int_{I\times I} n_\varepsilon(t,x)\ n_\varepsilon(t,y)\ dxdy \\ &\geq \Phi_m c^2 M_\varepsilon(t).\end{aligned}$$

Therefore, we obtain from (23)

$$\frac{d}{dt}M_\varepsilon(t) \leq \frac{M_\varepsilon(t)}{\varepsilon^2}\left(1 - c^2 M_\varepsilon(t)\Phi_m\right),$$

and again the upper bound follows directly. □

5.3 Estimates for the H.-J. Eq.

Theorem 5.3 *We assume (2), $\Phi \in W^{1,\infty}(\mathbb{R})$ and $M_\varepsilon(0) = M_0 < \infty$, and that φ_ε^0 and $\nabla\varphi_\varepsilon^0$ are bounded. Then, for all time $t > 0$, the solution to equation (4) satisfies the a priori bounds*

$$\|\varphi_\varepsilon(t,\cdot)\|_{L^\infty(0,1)} + \|\frac{\partial}{\partial x}\varphi_\varepsilon(t,\cdot)\|_{L^\infty(0,1)} \leq C(t),$$

and, after extraction of a subsequence, $\varphi_\varepsilon \to \varphi \in W^{1,\infty}\big((0,T)\times(0,1)\big)$ (uniformly locally in time) and (6) holds (in the viscosity sense).

Proof. Differentiating equation (4), we obtain the equation for $w = \nabla\varphi_\varepsilon$,

$$\frac{\partial w}{\partial t}(t) = \varepsilon\Delta w + 2\nabla\varphi_\varepsilon \cdot \nabla w - \nabla\Phi * n_\varepsilon. \tag{24}$$

Here, we can upper bound

$$|\nabla\Phi * n_\varepsilon(t)| \leq \|\nabla\Phi\|_\infty \bar{M}(t),$$

where $\bar{M}(t)$ is an upper bound of the total mass $M(s)$ for times $0 \leq s \leq t$ which is controlled thanks to Theorem 5.1. Therefore, by the maximum principle, we have

$$|w(t,x)| \leq \max_{x\in(0,1)} |w(t=0,x)| + \|\nabla\Phi\|_\infty \bar{M}(t)t.$$

This uniform estimate on the gradient gives a uniform estimate on φ_ε in $L^\infty\big((0,T)\times(0,1)\big)$ when coming back to the equation (4) because it boils down to heat equation with a bounded right-hand

side. And thus, the L^∞ bounds on φ_ε and $\frac{\partial}{\partial t}\varphi_\varepsilon$, as stated in Theorem 5.3, are proved.

Then we can obtain a local uniform L^2 estimate on $\frac{\partial \varphi_\varepsilon}{\partial t}$. To do that, we multiply for instance the equation (4) by $\frac{\partial \varphi_\varepsilon}{\partial t}$, and integrate. We obtain, denoting by C an absolute bound for $|\nabla\varphi_\varepsilon|^2+1-\Phi*n_\varepsilon$

$$\begin{aligned}\int_0^1 |\tfrac{\partial\varphi_\varepsilon(t)}{\partial t}|^2 dx &\leq \varepsilon \int_0^1 \tfrac{\partial\varphi_\varepsilon(t)}{\partial t}\Delta\varphi_\varepsilon(t) + C\int_0^1 |\tfrac{\partial\varphi_\varepsilon(t)}{\partial t}|dx \\ &\leq -\tfrac{\varepsilon}{2}\tfrac{d}{dt}\int_0^1 |\nabla\varphi_\varepsilon(t)|^2 dx + C\int_0^1 |\tfrac{\partial\varphi_\varepsilon(t)}{\partial t}|dx.\end{aligned}$$

Therefore, when integrating in time and using Cauchy-Schwarz inequality for the second term on the right, we find

$$\int_0^T\int_0^1 |\frac{\partial\varphi_\varepsilon(t)}{\partial t}|^2 dx \leq \frac{\varepsilon}{2}\int_0^1 |\nabla\varphi_\varepsilon(t=0)|^2 dx + C\sqrt{T}\left(\int_0^T\int_0^1 |\frac{\partial\varphi_\varepsilon(t)}{\partial t}|^2 dx\right)^{1/2}.$$

This proves a uniform bound on the quantity $\int_0^T\int_0^1 |\frac{\partial\varphi_\varepsilon(t)}{\partial t}|^2 dx$. Together with the bound on the x derivative, this proves the compactness of φ_ε for the uniform topology.

Passing to the limit in viscosity sense and almost everywhere is standard then. The constraint $\max\varphi(t,\cdot)=0$ follows from the mass constraint (see [11, 3, 22]). □

5.4 Numerical methods

We have used two different numerical schemes that we describe now. Both of them are very simple and based on finite differences.

In the first scheme, the discretization of equation (1) is based on a time splitting of the reaction term $n(1-\Phi*n)$ and the differential term. Considering a number N of points in x, we approximate the solution by a discrete vector n_i^k for $i=1,...,N$ and k the label for discrete time. We set $\Delta x = 1/N$ the space stepping and Δt the time stepping.

In order to avoid strong limitations on the time step, we use an exact resolution of the reaction term

$$n_i^{k+1/2} = n_i^k \exp\big(\frac{\Delta t}{\varepsilon}(1-\Phi*n^k)\big),$$

where the convolution $\Phi*n$ is computed according to

$$\Phi*n \approx \sum_{j=-J_M}^{J_M} \Phi_j n_{i-j},$$

where $J_M = b*N$. We use a three point implicit (or explicit when ε is small enough) scheme for the differential term

$$n_i^{k+1} = n_i^{k+1/2} + \frac{\varepsilon\,\Delta t}{2\Delta x^2}\,[n_{i+1}^{k+1} + n_{i-1}^{k+1} - 2n_i^{k+1}].$$

In the second scheme, we use an explicit scheme for the reaction as well as for the diffusion. The convolution is computed by using the trapeze formula:

$$\Phi*n \approx \sum_{j=0}^{J_M-1} (\Phi_j n_{i-j} + \Phi_{j+1} n_{i-j-1})/2 + (\Phi_{-j} n_{i+j} + \Phi_{-j-1} n_{i+j+1})/2.$$

This gives a better accuracy and allows to check that the number of discretization points is enough to resolve the singularities.

Finally, notice that for accuracy reasons it is necessary to ensure some kind of CFL condition

$$\frac{\Delta t}{\varepsilon} \ll 1. \tag{25}$$

This is imposed in order to ensure that the reaction term is well resolved. In practice we can choose $\frac{\Delta t}{\varepsilon} = .1$. As a consequence, when ε is small, the CFL condition for the diffusion term, namely

$$\frac{\varepsilon\, \Delta t}{2\Delta x^2} \leq 1,$$

can be achieved. Then the explicit scheme for the diffusion is stable.

References

[1] Atamas, S., Self-organization in computer simulated selective systems. Biosystems, 39 (1996), 143-151.

[2] Barles, G.; Evans, L. C. and Souganidis, P.E., Wavefront propagation for reaction diffusion systems of PDE, Duke Math. J. 61 (1990) 835-858.

[3] Barles, G. and Perthame, B., Concentrations and constrained Hamilton-Jacobi equations arising in adaptive dynamics. Work in preparation.

[4] Berestycki, H. and Hamel, F., *Reaction-Diffusion Equations and Propagation Phenomena*. Series Appl. Math. Sci., Springer, to appear.

[5] Carrillo, J.A., Cuadrado, S. and Perthame, B., Adaptive dynamics via Hamilton-Jacobi approach and entropy methods for a juvenile-adult model. Mathematical Biosciences, vol. 205(1) (2007), 137–161.

[6] Champagnat, N., Ferrière, R. and Méleard, S., Unifying evolutionary dynamics: from individual stochastic processes to macroscopic models. Theoretical Population Biology, 69 (2006), No. 3, 297-321.

[7] Crandall, M. G. and Lions, P.-L., User's guide to viscosity solutions of second order partial differential equations, Bull. Amer. Math. Soc. **27** (1992), 1–67.

[8] Darwin, C., *On the origin of species by means of natural selection*. John Murray, London, 1859. [1st edn].

[9] Desvillettes, L., Prevost, C. and Ferriere, R. Infinite Dimensional Reaction-Diffusion for Population Dynamics. Preprint n. 2003-04 du CMLA, ENS Cachan.

[10] Diekmann, O., Beginner's guide to adaptive dynamics, Banach Center Publications 63 (2004) 47-86.

[11] Diekmann, O., Jabin, P.-E., Mischler, S. and Perthame, B., The dynamics of adaptation : an illuminating example and a Hamilton-Jacobi approach, Th. Pop. Biol., 67(4) (2005) 257-271.

[12] Evans, L.C. and Souganidis, P.E., A PDE approach to geometric optics for certain semilinear parabolic equations. Indiana Univ. Math. J. 38 (1989), 141–172.

[13] Fleming, W.H. and Soner, H.M., Controlled Markov processes and viscosity solutions. Applications of Mathematics 25, Springer (1993).

[14] Génieys, S., Volpert, V. and Auger, P., Adaptive dynamics: modeling Darwin's divergence principle. C. R. Acad. Sc. Paris (2006).

[15] Geritz, S.A.H., Kisdi, E., Meszena, G. and Metz, J.A.J., Evolutionary singular strategies and the adaptive growth and branching of the evolutionary tree, Evolutionary Ecology 12 (1998) 35-57.

[16] Gourley, S.A., Travelling front of a nonlocal Fisher equation, J. Math. Biol. 41, 272–284 (2000).

[17] Hofbauer, J. and Sigmund, K., *Evolutionary games and population dynamics*. Cambridge University Press, Cambridge (1998).

[18] Kupiec, J.J. and Sonigo, P., *Ni Dieu ni gène. Pour une autre théorie de l'hérédité*. Seuil, Paris, 2000.

[19] Lefever, R. and Lejeune, O. On the origin of tiger bush. Bull. Math. Biology. 59(2) (1997) 263–294.

[20] Meinhardt, H., *Models of biological pattern formation*. Academic Press, London (1982).

[21] Murray, J.D., *Mathematical biology*, Vol. 1 and 2, Second edition. Springer (2002).

[22] Perthame, B., *Transport equations in biology*. Series 'Frontiers in Mathematics', Birkhauser (2006).

[23] Turing, A.M., The chemical basis of morphogenesis. Philosophical Transactions of the Royal Society **B 237** (1952), 37–72.